Mechanical Systems and Signal Processing 114 (2019) 146–164

Contents lists available at ScienceDirect

Mechanical Systems and Signal Processing

journal homepage: www.elsevier.com/locate/ymssp

Reliability of semi-active seismic isolation under near-fault earthquakes

Seda Öncü-Davas, Cenk Alhan *

Department of Civil Engineering, İstanbul University, Avcılar Campus, 34320 Avcılar, İstanbul, Turkey

ARTICLE INFO

Article history:
Received 1 August 2017
Received in revised form 26 March 2018
Accepted 29 April 2018

Keywords:
Monte-Carlo simulation
Semi-active control
Seismic base isolation
Structural reliability
Near-fault earthquakes

ABSTRACT

Structural control can be used for protecting buildings and its vibration-sensitive contents from earthquakes. Seismic isolation is a passive control system that lowers effective earthquake forces by utilizing flexible bearings. However, supplemental damping in the isolation system may become necessary to reduce large isolator displacements under near-fault earthquakes. Semi-active dampers are preferred over passive dampers because of their capacity in minimizing possible amplifications in floor accelerations due to increased damping. Semi-active dampers are also preferred over the active ones because of their higher stability and lower power consumption. On the other hand, seismic performance of semi-active isolation may vary due to variations in the mechanical properties of semi-active devices and/or seismic isolators. Such uncertainties alongside the uncertainties associated with ground motion parameters should be taken into consideration to develop a realistic picture of the behavior of seismically isolated buildings equipped with semi-active control devices. The objective of this study is to examine the effectiveness of semi-active isolation in protecting vibration-sensitive equipment and integrity of a structure by considering the aforementioned uncertainties and present the reliability of semi-active seismic isolation under near-fault earthquakes. For this purpose, this paper introduces a method that uses synthetically generated near-fault earthquakes and Monte-Carlo Simulations. This method is used to determine the reliability of a 3-story and a 9-story benchmark buildings with semi-active isolation systems under near-fault earthquakes of various magnitudes and varying fault distances. The results are presented in the forms of comparative plots of probability of failure and reliability.

1. Introduction

Structural control systems can be used in modern engineering practice to protect structures from destructive effects of earthquakes. Structural control systems are mainly categorized as passive, active, semi-active, and hybrid systems. The basic concept of passive control systems is to lower the effective earthquake forces by elongating the fundamental period of the structure, thereby, lowering both the floor accelerations and the inter-story drift ratios to keep them within desired limits. The main challenge that such systems face is the large displacement requirements of the isolation system in case of near-fault earthquakes [1], which may exceed practical and economical limits [2]. Such large base displacements may even exceed the seismic gap, thus, posing serious risks [3]. Providing high passive isolation damping may be of help but such a solution

* Corresponding author.
E-mail addresses: seda.oncu@istanbul.edu.tr (S. Öncü-Davas), cenkalhan@istanbul.edu.tr (C. Alhan).

https://doi.org/10.1016/j.ymssp.2018.04.045
0888-3270/

may cause increase in floor accelerations and inter-story drifts depending on the earthquake characteristics [4]. Various other studies [1,5–7] also revealed that additional damping that is necessary for controlling base displacement may not guarantee good performance in structural response under the near-fault earthquakes, which would be a problem for mission-critical buildings such as hospitals that house vibration-sensitive contents [2,8]. Thus, active or semi-active isolation systems that can adapt to earthquake excitations of different frequency contents are necessary. Although active control systems are effective, they require very high power to operate [9,10]. Moreover, adding mechanical energy actively to the building may cause stability problems to the structure [11–13]. These drawbacks increase the interest in semi-active control systems, which can provide the proper amount of damping without causing any stability problems. Also, they need much less power to operate than the active control systems [12,13]. Symans et al. [14] showed that both isolation displacement and superstructure response can be limited by such adaptive base isolation systems. Likewise, [15–17] confirmed that the safety performance of a seismic isolation system that is equipped with semi-active dampers are quite high and it is effective in simultaneously limiting both base displacement and superstructure responses.

On the other hand, it is known that the mechanical properties of isolators can vary due to the variation in temperature, ageing, contamination, or scragging [18–20]. Likewise, the mechanical properties semi-active control devices can vary. Researchers [18,19,21] have evaluated the effect of variability in passive isolation system parameters on the response of superstructure. The results emphasized the significance of variability of these parameters on the response of isolated buildings. At this point, it can be said that probabilistic seismic risk analysis, which takes such uncertainties into account, is the best method for determining the realistic seismic performance of seismically isolated buildings equipped with semi-active control systems. Due to the difficulty of describing the probabilistic characteristic of the whole problem analytically, the Monte-Carlo Simulation technique can be used as a convenient alternative. It is an accurate method for conducting safety and reliability analysis [22] that is based on mathematical modeling and recursive computer analysis in which the uncertainty is taken into account by defining random variables to follow certain probabilistic distributions.

The recent seismic risk studies on passive isolation systems and/or passive dampers [23] presented the seismic fragility of a high-rise reinforced concrete building retrofitted by means of viscous dampers with various effective damping ratios under synthetically developed ground motions. In order to evaluate the effectiveness of the external dissipation system, the seismic reliability analysis of a spherical storage tank with external metallic dampers was conducted by Curadelli [24]. Colombo and Almazán [25] assessed the seismic reliability of liquid storage tanks with external energy dissipation devices. The reliability analysis of the structure showed that the external energy dissipation system has the capability to reduce the probability of reaching the limit state by 81%. In another study conducted by Chakraborty and Debberma [26], the uncertainties in tuned liquid dampers were taken into consideration for the optimum design of these systems. Alhan and Gavin [8] presented the reliability of passive floor isolation systems for protecting vibration-sensitive equipment under synthetically developed earthquakes and concluded that for a reliable solution, semi-active isolation rather than passive one may be considered in case the structure is located in the close proximity of the fault line [27] evaluated the effect of the uncertainties in the properties of passive seismic isolators on the response of seismically isolated buildings by using Monte-Carlo Simulations. Although probabilistic seismic risk analysis relating to passive isolation systems and/or passive dampers has attracted great interest in recent years, there exist very few probabilistic research studies on seismically isolated buildings equipped with semi-active control systems in the literature. Among these, Chase et al. [28] compared the impact of a type of semi-active control strategy on the structural responses and evaluated the results in terms of statistical distributions. In order to determine the efficacy of smart damping technology, an energy-based probabilistic approach was presented by Aly and Christenson [29].

The objective of this study is to examine the effectiveness of semi-active isolation in protecting vibration-sensitive equipment and structural integrity by taking the uncertainties in the earthquake loading and the mechanical parameters of semi-active isolation systems into consideration and to present/evaluate the reliability of semi-active seismic isolation under near-fault earthquakes. For this purpose, the Monte-Carlo Simulations of benchmark buildings with semi-active isolation systems under synthetic near-fault earthquakes, which are generated for different magnitudes at various distances to the fault, are carried out and the results are presented in the form of comparative probability of failure and reliability plots. The mechanical parameters of semi-active isolation system including isolator stiffness, isolator damping, stiffness of semi-active control device and semi-active control device damping and the parameters of synthetic near-fault earthquakes including pulse period, pulse velocity, and decaying sinusoid damping factor are considered as random variables. 3-story and 9-story buildings are examined in order to take the influence of superstructure flexibility into account. Nonlinear time history analyses are conducted using the modified version of 3D-BASIS [30] that is capable of analyzing three-dimensional seismically isolated buildings equipped with semi-active control devices [31]. This modified version is further modified by [32] in order to add the capability for carrying out recursive Monte-Carlo analyses. The random values for uncertain parameters following specific probabilistic distributions are obtained via MATLAB [33] for use in 3D-BASIS.

The organization of the text is as follows: First the structural modeling concept that combines the superstructure, isolation system and semi-active devices are given, then the synthetic earthquake pulse model is summarized. In the third section, a short description of the application of Monte-Carlo Simulation is given, which is followed by the descriptions of random variables and probability distributions used in this study. Finally, results are presented in the forms of comparative plots of probability of failure and reliability along with performance tests that reveal the success of semi-active isolation in near-fault regions considering practical and economical limits.

2. Structural model

3-story and 9-story benchmark building models are used in this study. Each model consists of two main parts: 3-dimensional shear building superstructure and semi-active base isolation system that consists of rubber bearings and semi-active control devices (Fig. 1). The superstructure plan is symmetric and floor masses are assumed to be the same and lumped at the center of the gravity of each floor level. The story stiffness values are assumed to be the same and adjusted

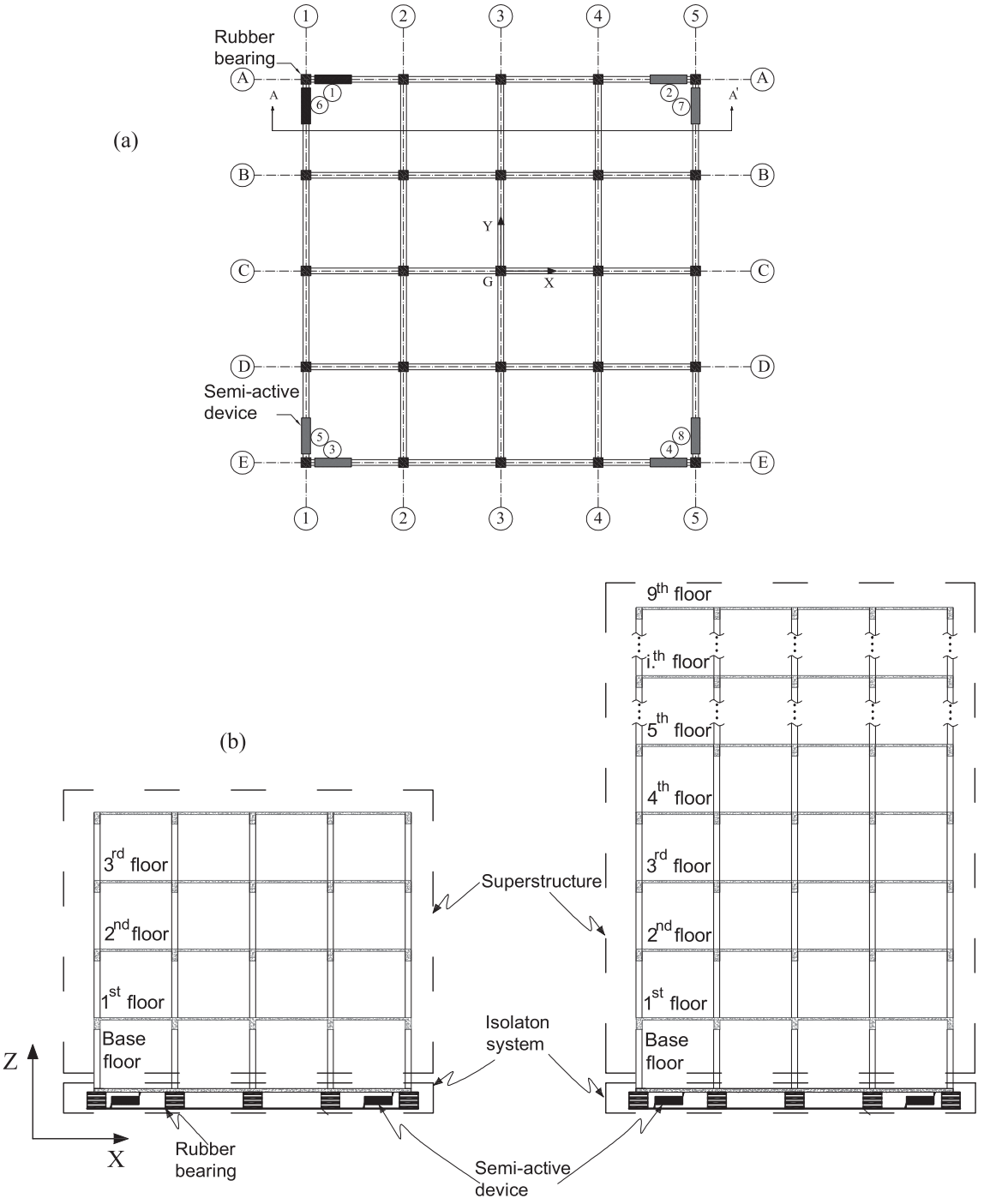

Fig. 1. Benchmark 3-story and 9-story buildings: (a) plan view, (b) sectional view.

to provide fundamental fixed-base periods of 0.34 s and 0.91 s for the 3-story and 9-story model, respectively. The superstructure modal damping ratio is considered as 5% of critical for all modes in each of these models.

Isolation system consists of 25 rubber bearings located under each column and 8 semi-active control devices that are placed at each corner of the isolation system in both orthogonal directions (Fig. 1). Rubber bearings are modeled to represent smooth bilinear hysteretic behavior [30]. It adopts Park et al. [34] which is essentially the extended version of Bouc-Wen model [35,36] and takes biaxial interaction into account. In this model, the forces developed in the bearings in two orthogonal directions depend on the yield force, yield displacement, post-yield to pre-yield stiffness ratio. The mathematical details can be found elsewhere [30].

The isolation periods of the benchmark buildings are obtained based on the total weights of the buildings (W) and the total post-yield stiffness (K_{2t}) of the isolation systems as given in Eq. (1).

$$T_0 = 2\pi\sqrt{W/(gK_{2t})} \tag{1}$$

where g is the gravitational acceleration. The total weights (W) of the benchmark models are 12,557 kN and 31,392 kN, respectively. The nominal total post-yield stiffness (K_{2t}) can be calculated for each model to provide an isolation period that is assumed as 4 s for both buildings. The nominal total pre-yield stiffness (K_{1t}) is obtained afterwards by the following equation in which Q_t is the nominal total characteristic force and D_y is the nominal yield displacement which is assumed as 20 mm in this study.

$$K_{1t} = Q_t/D_y + K_{2t} \tag{2}$$

To determine the nominal total characteristic force of Q_t, the nominal total yield strength ratio (Q_t/W) is taken as 10%. Several studies (e.g. [37–40]) show that the characteristic strength ratio typically varies between 5% and 15%. Therefore, a value of 10% is chosen as it represents a typical average value. Once the nominal total post-yield stiffness and the nominal total pre-yield stiffness values are calculated, the nominal total yield strength (F_{yt}) and the nominal post-yield to pre-yield stiffness ratio (α) can be obtained by Eqs. (3) and (4), respectively.

$$F_{yt} = K_{1t}D_y \tag{3}$$

$$\alpha = K_{2t}/K_{1t} \tag{4}$$

Then, by dividing K_{1t}, K_{2t} and F_{yt} by the total number of isolators, 25, the nominal pre-yield stiffness K_1, the nominal post-yield stiffness K_2, and the nominal yield strength F_y are obtained for each individual rubber bearings. The nominal post-yield to pre-yield stiffness ratio (α) and the nominal yield displacement (D_y) would be the same for both the isolation systems and each individual isolator for the nominal case.

The other main part of the isolation system is the semi-active control device which is basically a controllable Maxwell element. As detailed in Fig. 2, the element consists of a spring that is connected in series with a controllable damper.

The modeling details of a semi-active device which is essentially a controllable Maxwell element is provided in [31] comprehensively and will be summarized here. The semi-active control device is modeled to follow the bang-bang pseudo-skyhook control rule [42]:

$$u = H(f_d \cdot V_a) \tag{5}$$

where u is the control signal, $H(.)$ is the Heaviside step function, f_d is the control force, and V_a is the absolute device velocity. The control rule provides the most suitable damping by turning the damper on or off. The control rule decides to minimize

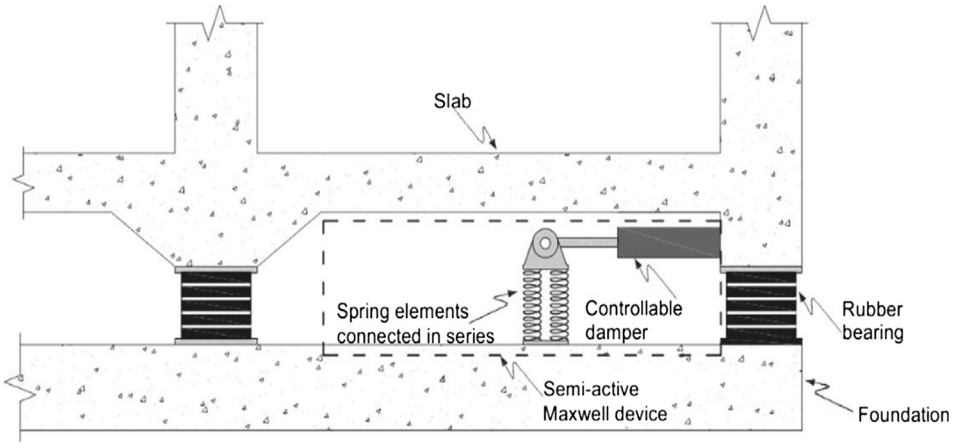

Fig. 2. Maxwell element (adapted from Vu et al. [41]).

the damping of semi-active device ($u = 0$) in case $f_d.V_a \leq 0$. Otherwise, u is set to 1 and damping is maximized. As seen in Eq. (6), the controllable device damping ($c_d(u)$) depends on the control signal (u) and changes according to the control signal value.

$$c_d(u) = c_{\min}(1-u) + c_{\max}u \tag{6}$$

in which, c_{min} and c_{max} are minimum and maximum damping, respectively. The control force of the device is calculated by Eq. (7), which is dependent on the controllable device damping ($c_d(u)$), the stiffness of device (k_d), and the relative velocity of the device ($\dot{r}_d$) where an over-dot stands for time derivative d/dt.

$$\dot{f}_d = -\frac{k_d}{c_d(u)} f_d + k_d \dot{r}_d \tag{7}$$

3. Synthetic earthquake pulse model

In recent years, there has been an increased interest in studies on seismically isolated buildings under near-fault earthquake pulses, which are commonly observed in ground motion records obtained in distances within 10.0 km from the fault [43]. Since the number and variety (in terms of magnitude and fault-distance) of historical near-fault earthquake records are not enough for use in numeric simulations, various researchers [44–51] developed different analytical pulse models that represent pulse-like near-fault ground motions. In this study, Agrawal and He [47] pulse model is used since it both has the capability of representing typical near-fault ground motions and is formed of a simple mathematical expression. Agrawal and He [47] pulse model is a special case of He and Agrawal [50] model. Since near-fault earthquakes involve decaying sinusoids and combinations thereof, the velocity time history is defined as a decaying sinusoid function which is generated by the following closed-form approximation:

$$v(t) = s e^{-\zeta_p \omega_p t} \sin \omega_p \sqrt{(1-\zeta_p^2)}\, t \tag{8}$$

By differentiating Eq. (8), the ground acceleration is obtained as:

$$a(t) = s e^{-\zeta_p \omega_p t}\left[-\zeta_p \omega_p \sin \omega_p \sqrt{(1-\zeta_p^2)}\, t + \omega_p \sqrt{(1-\zeta_p^2)} \cos \omega_p \sqrt{(1-\zeta_p^2)}\, t\right] \tag{9}$$

where ζ_p is the damping factor of the decaying sinusoid. In order to generate near fault earthquakes with a peak ground velocity (υ_p), a pulse period (T_p), and a decaying factor (ζ_p) to emulate the corresponding pulse model, the initial amplitude of the pulse (s) and the frequency of the sinusoid (ω_p) can be calculated by the following equations as suggested by Dicleli and Buddaram [37]:

$$\omega_p = 2\pi \Big/ \left[T_p \sqrt{(1-\zeta_p^2)}\right] \tag{10}$$

$$s = \upsilon_p \Big/ \left[e^{-\zeta_p \omega_p t_p} \sin \omega_p \sqrt{(1-\zeta_p^2)} t_p\right] \tag{11}$$

Here, t_p is the time at which the peak velocity occurs and is calculated by equating Eq. (9) to zero and solving for t.

In order to generate earthquake pulse time histories at specific closest fault distances (r) for earthquakes of specific moment magnitudes (M_w) [37], the peak ground velocity (υ_p) and the pulse period (T_p) are calculated via Eqs. (12) and (13) proposed by [52].

$$\log_{10}(\upsilon_p) = -1.0 + 0.5M_w - 0.5\log_{10}(r) \tag{12}$$

$$\log_{10}(T_p) = -2.5 + 0.425M_w \tag{13}$$

In this study, the earthquake pulse models are simulated for the closest fault distances of r = 3 km, 6 km and 9 km and the earthquake magnitudes of M_w = 6.5, 6.75, 7.0, and 7.25 and combinations thereof. The nominal values of the pulse velocity (υ_p) and the pulse period (T_p) are calculated using Eq. (12) and (13) according to the aforementioned r and M_w parameters and are listed for each combination in Table 1. The nominal value of the other parameter, i.e. decaying sinusoid damping

Table 1
Nominal values of the parameters of near-fault ground motions for different moment magnitudes and fault distances.

r (km)	M_w	T_p (s)	υ_p (cm/s)	ζ_p (%)	r (km)	M_w	T_p (s)	υ_p (cm/s)	ζ_p (%)	r (km)	M_w	T_p (s)	υ_p (cm/s)	ζ_p (%)
3	6.5	1.83	102.67	20	6	6.5	1.83	75.6	20	9	6.5	1.83	59.28	20
	6.75	2.33	136.91	20		6.75	2.33	96.81	20		6.75	2.33	79.05	20
	7.0	2.99	182.57	20		7.0	2.99	129.1	20		7.0	2.99	105.41	20
	7.25	3.81	243.47	20		7.25	3.81	172.16	20		7.25	3.81	140.57	20

factor (ζ_p) required to produce the synthetic near-fault earthquake pulses is considered as 20% since most (50%) of the recorded near-fault earthquakes contain forward and backward velocity pulses that correspond to the decaying sinusoid damping factor of 20% [53].

4. Application of Monte-Carlo simulation

Monte-Carlo simulation is a convenient method for determining the reliability of engineering systems (see [54] for a complete discussion) in which the parameters with uncertainties are defined as random variables. Each random parameter is generated to follow a certain probability distribution that is compatible with its nature. To do so, first uniformly distributed random numbers, which vary between 0 and 1, are produced. Then, by using the inverse cumulative distribution function (CDF) method, the numbers are transformed into random numbers with a characteristic of the desired distribution. First, uniformly distributed random numbers (u_i) are generated for uniformly distributed random variables (U). Then, CDF of each random variable value (x_i), which corresponds to random variable X, is equated to u_i and the equation is solved to obtain x_i. A probability distribution specifies the probability (or the probability density in the case of continuous random variables) of the random variable X taking the value x_i. There are various distribution functions including but not limited to normal, log-normal, uniform, Weibull, or exponential. Normal and Weibull distributions, which are frequently used in applied engineering problems, are used here as they are suitable for the random parameters defined in this study.

The normal distribution is specified by its cumulative density function, F_x, that is indicated in Eq. (14). CDF provides the knowledge of probability that a continuous or discontinuous random variable is equal to or less than a certain value (x_i). The shape of the normal distribution depends on two parameters that reveal the mean of the random variable (μ_x) and standard deviation of it (σ_x). A standardized measure of dispersion with respect to the mean value is defined as the coefficient of variation ($c.o.v._x$) and is calculated by $c.o.v._x = \sigma_x/\mu_x$. It also provides an information about the skewness of the dispersion. If it takes a small value, a small/low uncertainty is associated with that variable [55].

$$F_x(x) = \int_{-\infty}^{x} \frac{1}{\sigma_x\sqrt{2\pi}} e^{-\frac{(x-\mu_x)^2}{2\sigma_x^2}} dx \tag{14}$$

The CDF function of the continuous random variable (X) with a Weibull distribution is given in Eq. (15).

$$F_x(x) = 1 - e^{\left(-\frac{x}{\gamma_x}\right)^{k_x}} \tag{15}$$

Here, k_x is the shape parameter that alters the variation of the random variable and γ_x is the shape (scale) parameter that changes the form of the probability distribution function (PDF) of the random variable.

After the values of the random variables are generated – as much as the required number of simulations (n_{mcs}) – to follow their specific probability distributions, the problem is evaluated deterministically for each set of realization of all random variables. This phase is also known as numerical experimentation. Finally, probabilistic information is extracted from the results of these numerical experiments [55]. A comprehensive example that depicts the application of all steps of a Monte Carlo Simulation can be found in [56].

5. Random variables and probability distribution functions

If a problem has the character of randomness in its constituent parameters, it has more than one possible outcome. Quantifying the uncertainties in the problem is the first stage in which the effect of potential variability is taken into account. In this context, this study considers the uncertainties in the parameters of the semi-active isolation system and synthetic earthquake parameters. Accordingly, synthetic earthquake parameters of ζ_p, T_p, and υ_p are considered as random variables. In order to describe the distributions of the pulse period (T_p) and the maximum pulse velocity (υ_p), the Weibull distribution is considered/deemed suitable. As mentioned in Section 3, the near-fault ground motion pulses are produced by considering various deterministic values of the moment magnitude of the earthquake (M_w) and the closest distance to the fault (r) in order to examine how the probabilities of failure and probabilistic seismic performance vary with respect to these variables. As shown in Table 1, the nominal values of ζ_p, T_p, and υ_p corresponding to deterministic values of M_w and r are calculated via Eqs. (12) and (13). A normal distribution with a mean value of 0.2 and covariance of 15% is applied for the decaying sinusoid damping factor (ζ_p). Fig. 3(j) should be referred to see how the covariance values of 10, 15, and 20% yields different values of ζ_p and how 15% is more suitable than others in order to attain physically realistic values.

The characteristic mechanical properties of the rubber isolators α, F_y, and D_y are also considered as random variables. Likewise, the characteristic properties of semi-active control device, i.e. k_d, c_{max}, and c_{min} are modeled as random variables. All of the isolation system parameters are assumed to follow a normal distribution with a coefficient of variation ($c.o.v._x$) of 10%, which is typical for most engineering system parameters. The nominal (mean) values of the parameters for the 3-story and 9-story buildings are given in Table 2.

The probability distribution of a random variable can be defined by its probability density function (PDF). The probability distributions of the considered semi-active isolation system random variables, which belong to 3-story and 9-story buildings, can be defined by their probability density function (PDF). The PDFs of the considered semi-active isolation system ran-

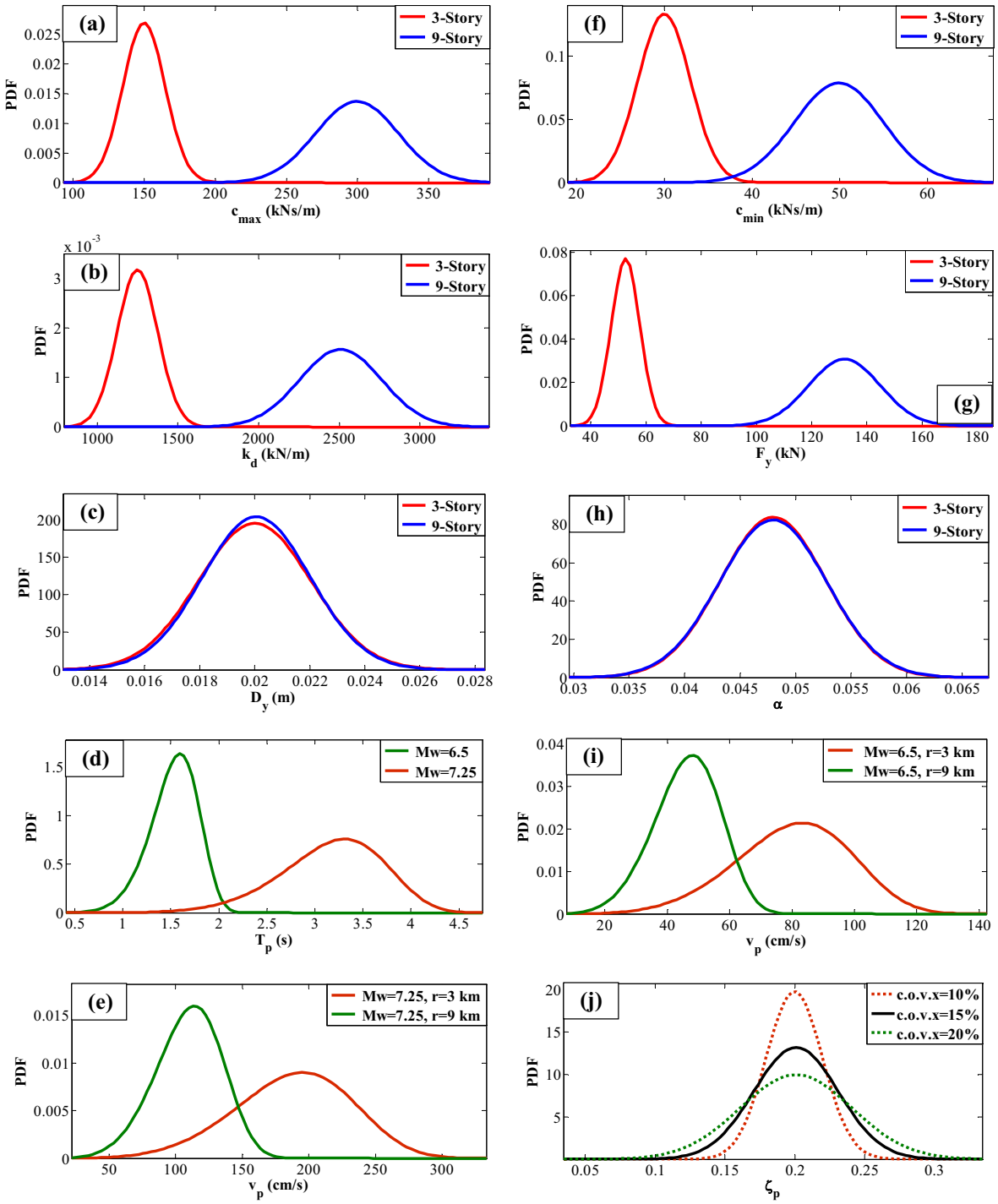

Fig. 3. The PDFs of random variables: (a)–(c) and (f)–(h) for the semi-active isolation system parameters, and (d), (e), (i), (j) for the synthetic earthquake parameters.

Table 2
Nominal values of the mechanical parameters of the rubber bearings and the semi-active device properties.

Model	α	F_y (kN)	D_y (m)	k_d (kN/m)	c_{max} (kNs/m)	c_{min} (kNs/m)
3-story	0.048	52.754	0.02	1250	150	30
9-story	0.048	131.89	0.02	2500	300	50

dom variables are obtained via MATLAB and are depicted in Fig. 3(a)–(c) and (f)–(h). Once the random variables of the α, F_y, and D_y for the rubber isolators are generated, the other variables K_1, K_2, and Q that are inter-related to these variables are obtained by Eqs. (2)–(4). The PDFs of the decaying sinusoid factor (ζ_p), the pulse period (T_p), and the maximum pulse velocity (υ_p) are shown in Fig. 3(d), (e), (i), and (j).

6. Results

Since this study is a numerical-intensive study, selecting the optimum number of simulations to be performed is important. For this reason, a preliminary study has been carried out to determine the optimum number of Monte-Carlo simulations (n_{mcs}). It was determined that variation in P_f values obtained for different cases ceased for approximately $n_{mcs} \geq 3000$. Monte-Carlo simulations have been performed with $n_{mcs} = 3000$ samples for each case which required a total of 72,000 bidirectional nonlinear time history analyses of the benchmark 3-story and 9-story seismically isolated buildings equipped with semi-active control systems under random synthetic ground motions of different characteristics. It is important to mention that n_{mcs}, here, stands for the number of Monte-Carlo simulations. Fig. 4 depicts sample velocity time histories of the random synthetic earthquakes for different magnitudes and closest fault distances that are used in the Monte-Carlo simulations. Each figure consists of plots corresponding to nominal case where T_p, υ_p, and ζ_p attain nominal values (see Table 2) and deviated cases where each parameter deviates by ±10%.

6.1. Cumulative distribution function plots

First, cumulative distribution function (CDF) plots of peak story drift ratios (psdr), peak floor accelerations, and peak base displacements are constructed for different earthquake magnitudes at various fault distances. The CDF plots can be used to conveniently determine any reliability level as they conveniently provide the probability of exceedance corresponding to any chosen limit state value. The probabilities of failure obtained by making use of these plots are discussed in detail in the proceeding subsection. Due to the limited space, here CDF plots of peak top floor accelerations (ptfa) and peak base displacements (pbd) corresponding to the lowest and highest earthquake magnitude cases ($M_w = 6.5$ and 7.25) at different closest fault distances are given only in Figs. 5 and 6 for both the 3-story and 9-story buildings, respectively. It is impressive to see how the CDF curves differ and the probabilities of failure increase as the earthquake magnitude increases, the closest fault distance decreases and the number of stories increases.

As seen from Fig. 5(a) and (b), peak top floor accelerations depending on the closest fault distances (r) can change from 0.92 m/s^2 to 3.38 m/s^2 for $M_w = 6.5$ earthquake, while they attain values between 1.02 m/s^2 and 9.08 m/s^2 in case of the $M_w = 7.25$ earthquake for the rigid low-rise (3-story) building. As seen from Fig. 5(c) and (d), peak base displacements depending on the closest fault distances (r) can change from 0.021 m to 0.63 m for the $M_w = 6.5$ earthquake and from 0.032 m to 2.78 m for the $M_w = 7.25$ earthquake for the 3-story building. For the building with a more flexible superstructure (9-story), the upper limit values of ptfa increase up to 7 m/s^2 and 9.4 m/s^2 for the $M_w = 6.5$ and $M_w = 7.25$ earthquakes, respectively while they do not change significantly in terms of peak base displacement.

6.2. Probabilities of failure

Limit state functions, i.e. the performance limits for the seismically isolated benchmark buildings equipped with semi-active control devices have to be defined first to determine the probabilities of failure. In this study, three seismic response parameters are considered: peak floor accelerations which can be directly related to the safety of vibration-sensitive equipment [57], peak story-drift ratios which can be directly related to the safety of both structural and non-structural elements such as partition walls, and windows [58], and peak base displacement which can directly be related to the safety of the isolation system and hence, the integrity and safety of the superstructure [59]. A comprehensive discussion of the practical limits of peak floor accelerations and peak base displacement for different performance objectives are provided by Alhan and Öncü-Davas [2] and similar performance limits are considered in this study corresponding to the most stringent, the moderate, and the least stringent cases: $La_1 = 3$ m/s^2, $La_2 = 5$ m/s^2, and $La_3 = 10$ m/s^2 are the three considered levels of peak floor acceleration limits, which may account for different tolerable limits of various vibration-sensitive equipment for operating or non-operating conditions. $Ld_1 = 40$ cm, $Ld_2 = 70$ cm, and $Ld_3 = 100$ cm are the three considered levels of peak base displacement performance limits with Ld_1 corresponding to a very economical design capacity in case of near-fault earthquakes and Ld_3 corresponding to the typical rubber-based isolator capacity.

Since peak inter-story drift ratio is an indicative response parameter regarding the safety of structural and non-structural elements, there exist clear code limitations to this seismic response parameter. ASCE 7–10 [60] specifies that the peak story inter-drift ratio of a seismically isolated building shall not exceed 0.02. But, when the secondary effects of the isolation system are ignored, this limit is decreased to 0.01 by the code, which is the typically preferred limit in practice. According to [61], 0.01 represents the limit where accidental yielding can occur and 0.005 represents the limit corresponding to the elastic behavior of the superstructure. For avoiding damage to brittle non-structural members, 0.0025 can be considered as the most stringent limit. Consequently, the inter-story drift ratio performance limits considered in this study are $Ldr_1 = 0.0025$, $Ldr_2 = 0.005$, and $Ldr_3 = 0.01$.

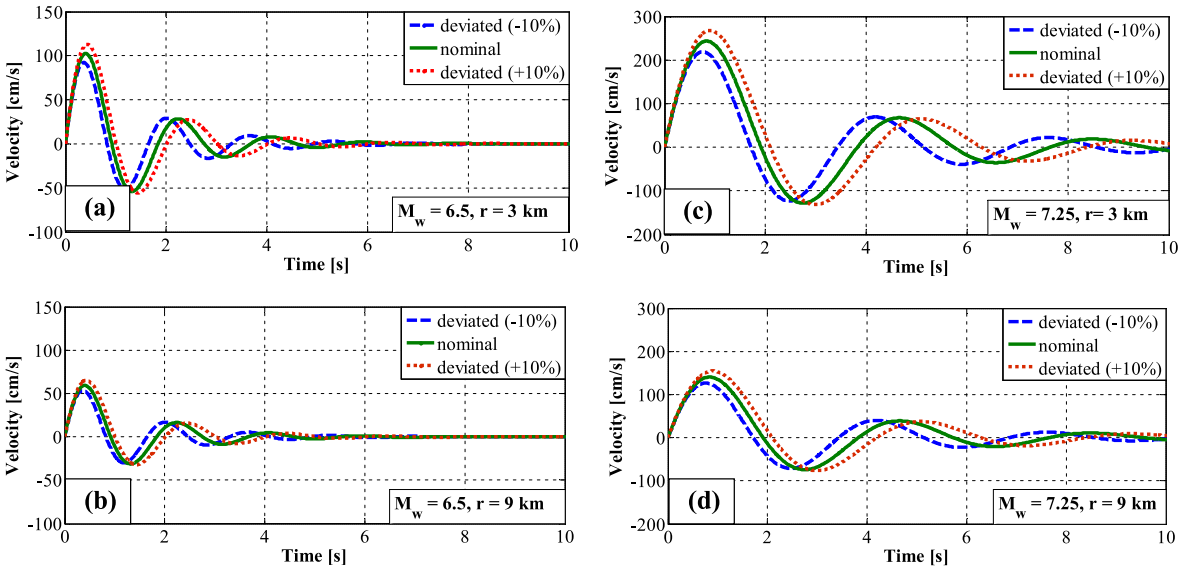

Fig. 4. Sample velocity time histories of the random synthetic earthquakes for different magnitudes and closest fault distances corresponding to nominal T_p, υ_p, and ζ_p values and 10% deviated cases.

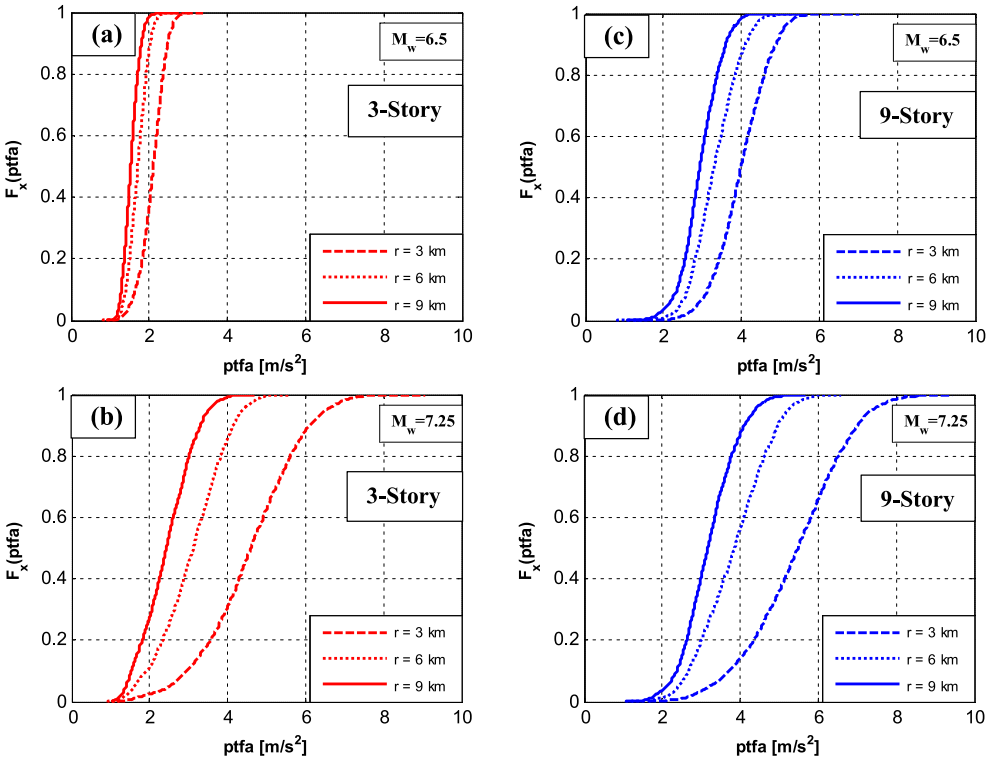

Fig. 5. Cumulative distribution function plots of peak top floor acceleration.

Once the performance limits are set as described above, the limit state functions ($g(X)$) can be specified. For instance, for the ith floor, the performance limit state function corresponding to the peak floor acceleration limit of $La_1 = 3$ m/s^2 can be defined as

$$g(X) = 3 - \text{peak i}^{\text{th}} \text{ floor acceleration} \tag{16}$$

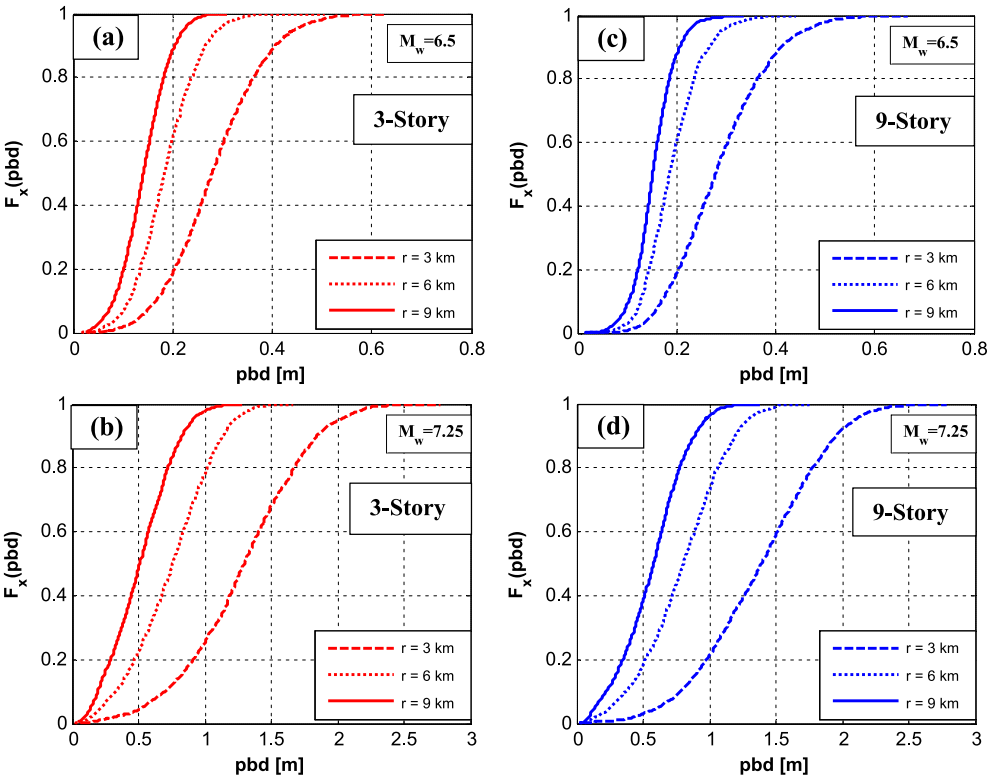

Fig. 6. Cumulative distribution function plots of peak base displacement.

and the conditions where the limit state function is equal to or less than 0 indicate the failure state ($g(X) \leq 0$). Then, the probability of failure (P_f) is calculated by dividing the number of simulations where $g(X) \leq 0$ exceeding the determined limit state ($n_{[g(X)\leq 0]}$) by the total number of simulations n_{mcs}.

$$P_f = \frac{n_{[g(X)\leq 0]}}{n_{mcs}} \tag{17}$$

The probability of failure (P_f) profiles in terms of the peak floor accelerations and the peak story-drift ratios of the 3-story and 9-story semi-actively isolated buildings at different fault distances and for different earthquake magnitudes are obtained for the most stringent and the moderate performance limits along the height of the building (0 represents the base floor) and given in Figs. 7–10. Since all probabilities of failure in terms of the peak floor accelerations and the peak story-drift ratios are obtained as 0% for the least stringent performance limits, the probability of failure plots for these performance limits are not presented. Finally, Fig. 11 depicts the probabilities of failure in terms of peak base displacement for all performance limits.

As a general trend, the probabilities of failure (P_f) significantly increase as the moment magnitude increases and the fault distance decreases. The probabilities of failure in terms of peak floor accelerations and peak story-drift ratios are observed to be much larger for the more flexible superstructure, i.e. 9-story building, while they do not differ significantly between the 3-story and 9-story buildings in terms of peak base displacements. In addition, it is observed that the probabilities of failure in terms of peak floor accelerations and the peak story-drift ratios vary along the height of the building in case of flexible superstructure (i.e. 9-story building) whereas they do not change much from floor to floor in case of rigid superstructure (i.e. 3-story building). Figs. 7–11 provide a wide spectrum of probabilities of failure, which can be used to determine the reliability levels for any required case.

For the moderate acceleration performance limit ($La_2 = 5$ m/s^2) the probabilities of failure in all floors of the 3-story building are practically zero for earthquakes with $M_w \leq 7.0$ at all closest fault distances (Fig. 7(a)–(c)). Only for $M_w = 7.25$ and $r = 3$ km P_f increases to about 38% (Fig. 7(d)). Although higher probabilities of failure are observed the for 9-story building, they are still in a tolerable range with P_f less than about 25% for earthquakes with $M_w \leq 7.0$ (Fig. 7(e)–(g)). The highest P_f is observed for $M_w = 7.25$ and $r = 3$ km where it slightly exceeds 60% at the top floor (Fig. 7(h)). For the most stringent acceleration performance limit ($La_1 = 3$ m/s^2) the probabilities of failure increase to an unacceptable level for the 3-story building in the worst case scenario of $M_w = 7.25$ and $r = 3$ km where P_f increases up to about 90% for all floors (Fig. 8(d)). More significant increases in P_f are observed at the upper-most and lower-most floors of the 9-story building where it goes up to 90% (Fig. 8(e)–(h)) while it is almost zero for mid-floors at all closest fault distances for earthquakes with $M_w \leq 6.75$ (Fig. 8(e)–(f)), except for $M_w = 6.75$, $r = 3$ km. For the least stringent acceleration performance limit ($La_3 = 10$ m/s^2), the probabilities of

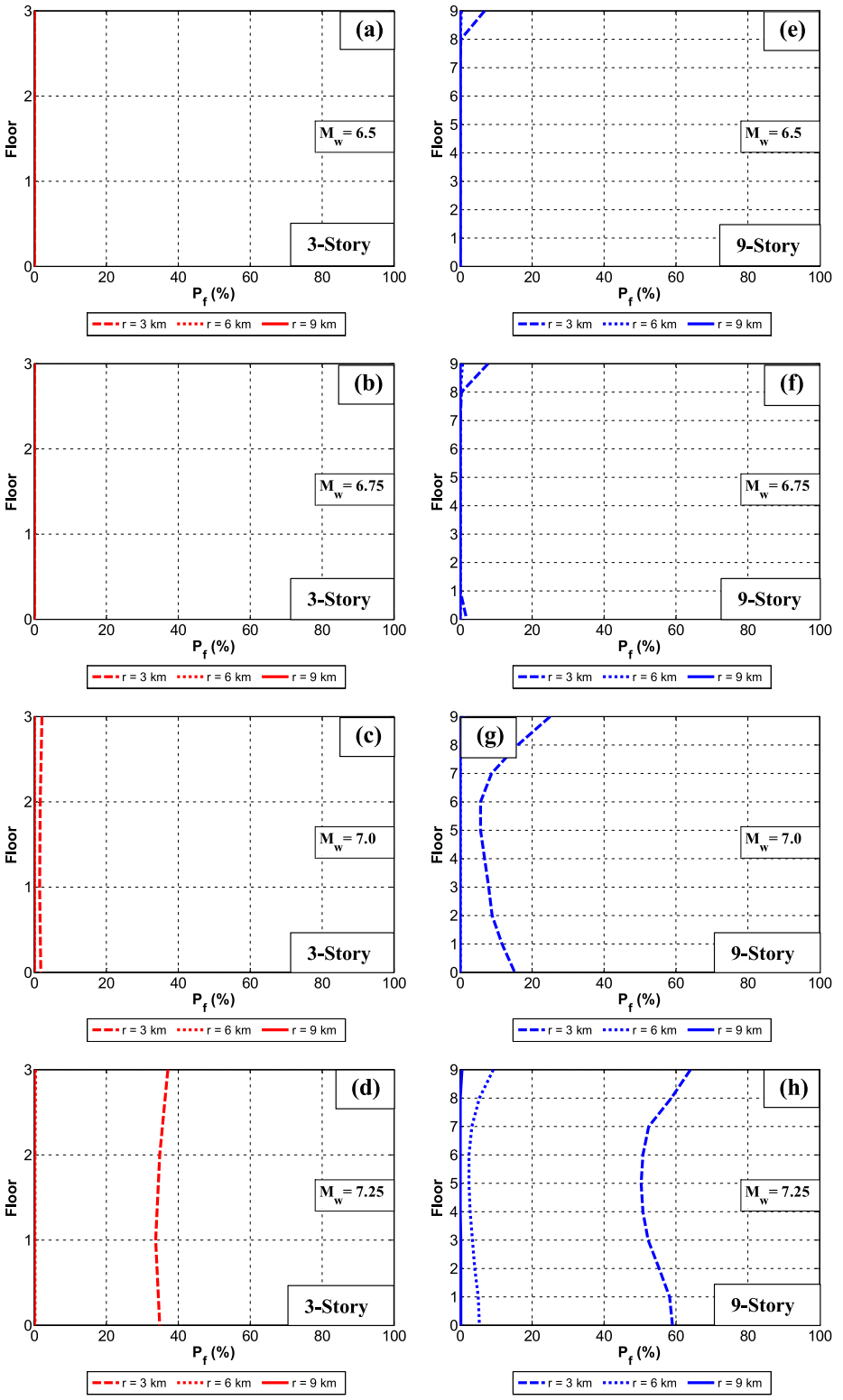

Fig. 7. Probability of failure profiles in terms of peak floor acceleration for the moderate limit of $La_2 = 5$ m/s^2.

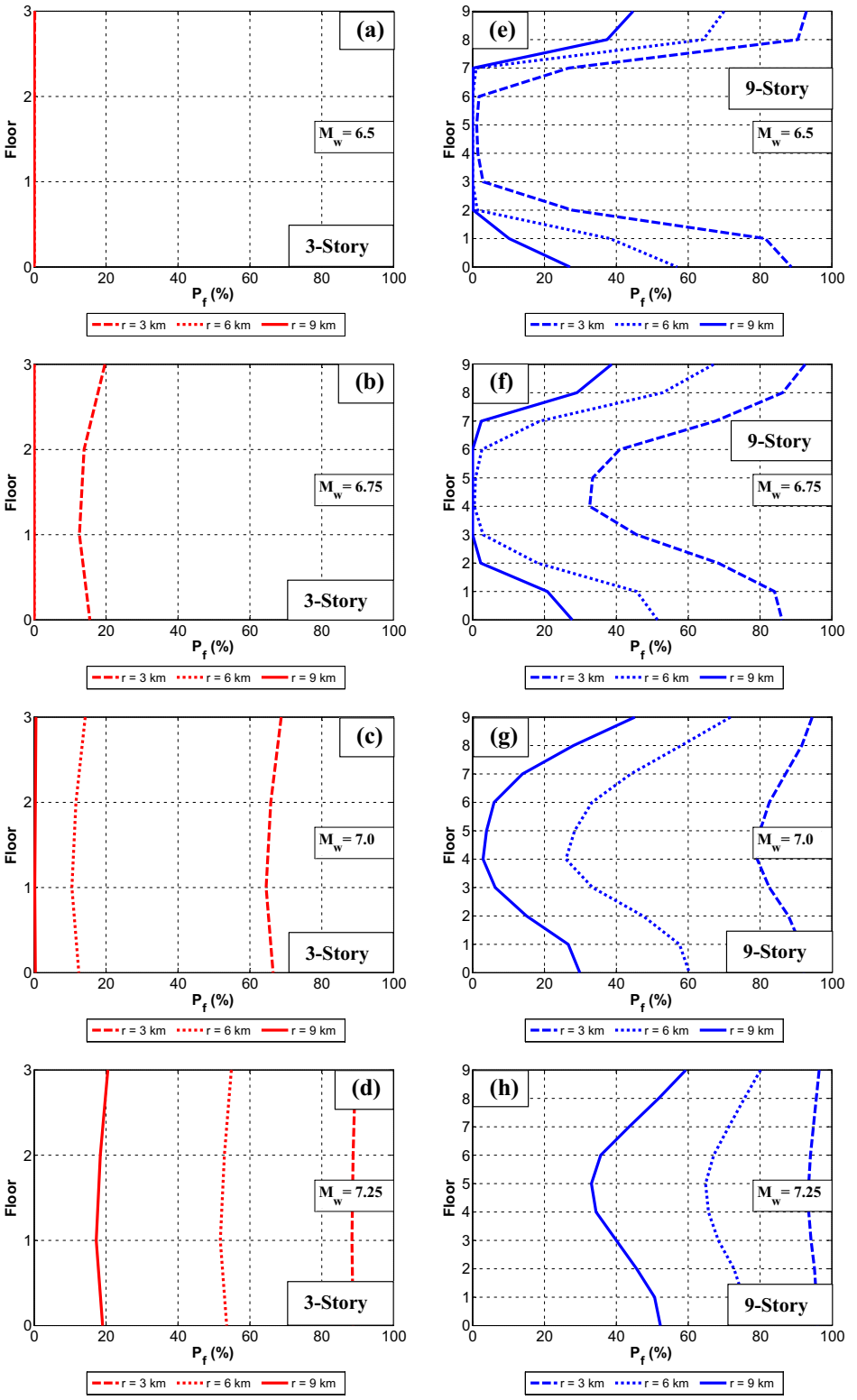

Fig. 8. Probability of failure profiles in terms of peak floor acceleration for the most stringent limit of La_1 = 3 m/s^2.

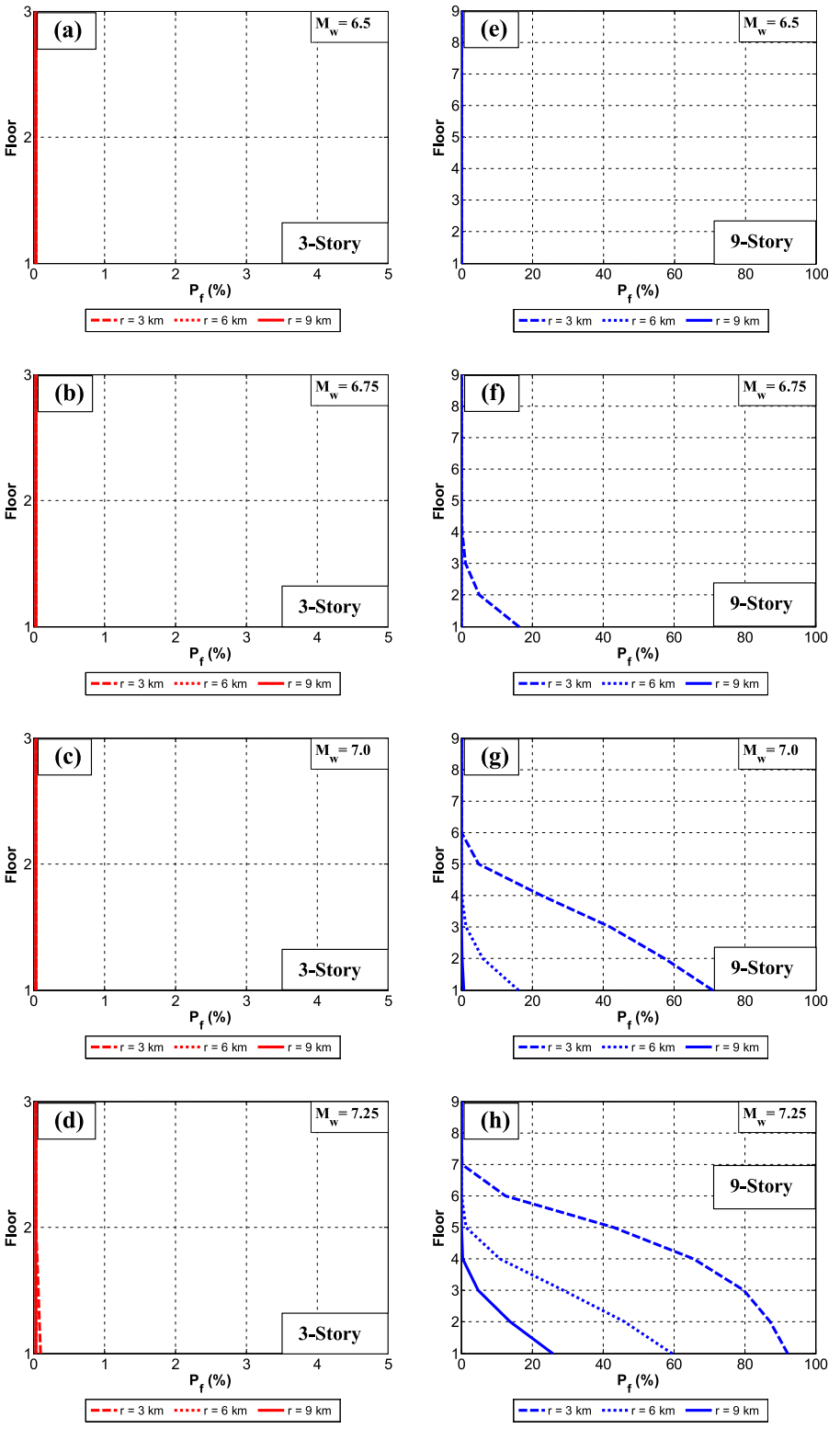

Fig. 9. Probability of failure plots in terms of story-drift ratio for the moderate limit of $Ldr_2 = 0.005$.

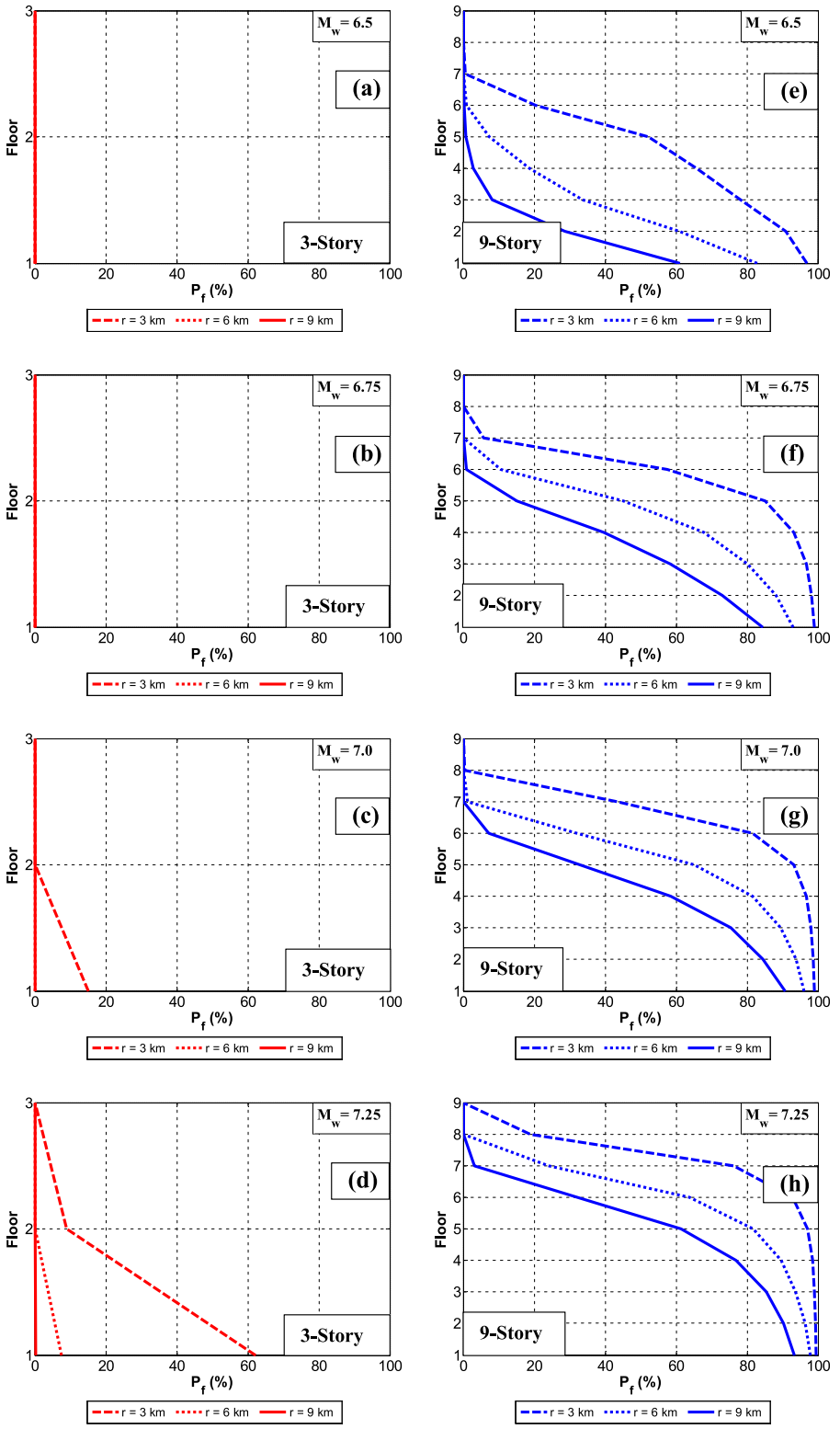

Fig. 10. Probability of failure plots in terms of story-drift for the most stringent limit of $Ldr_1 = 0.0025$.

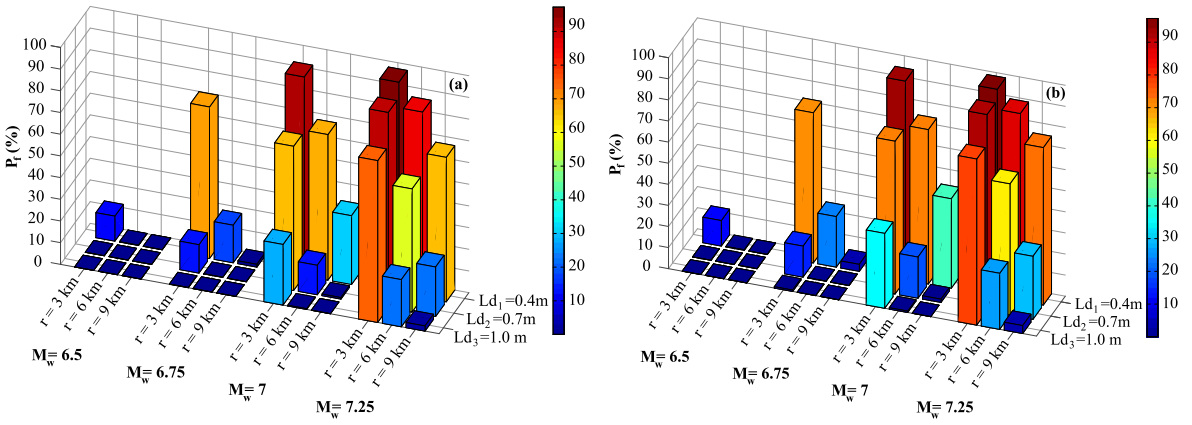

Fig. 11. Probability of failure plots in terms of peak base displacement for all performance limits (Ld_1 = 0.4 m, Ld_2 = 0.7 m and Ld_3 = 1.0 m): 3-story (a) and 9-story building (b).

failures for both 3-story and 9-story buildings are practically 0% for all earthquake magnitudes at all closest fault distances. Therefore, corresponding probability of failure plots are not presented here.

For the moderate peak story-drift ratio performance limit (Ldr_2 = 0.005), probabilities of failure for all earthquake moment magnitudes and all closest fault distances are about zero for the 3-story building (Fig. 9(a)–(d)). A very close performance is observed for the most stringent peak story-drift ratio performance limit (Ldr_1 = 0.0025) with P_f being about zero for all cases (Fig. 10(a)–(d)), except for the bottom story in case of M_w = 7.0 and r = 3 km where it is observed to be 18% (Fig. 10(c)) and M_w = 7.25 and r = 3 km where it is observed to be 60% (Fig. 10(d)). But for the 9-story building, the probabilities of failure increase as the earthquake magnitude increases and closest fault distance decreases (Figs. 9(e)–(h) and 10(e)–(h)). In particular, the probabilities of failure of the lower-most floors are observed to be higher which can go up to 90% in case of M_w = 7.25 and r = 3 km with Ldr_2 = 0.005 (Fig. 9(h)) and 90% to 100% in case of M_w = 7.25 and all closest fault distances with Ldr_1 = 0.0025 (Fig. 10(h)). For the least stringent limit (Ldr_3 = 0.01), P_f for all buildings are practically 0% for all M_w, r and thus corresponding plots are not presented here.

In order to make a visual comparison between the rigid 3-story and the flexible 9-story building in terms of probabilities of failure considering peak base displacements, comparative plots are given in Fig. 11 for all moment magnitudes and all closest fault distances subject to the three peak base displacement performance limits. This figure shows that the probabilities of failure for each building are similar. The probabilities of failure are practically zero even in the close vicinity of the fault (r = 3 km) for the M_w = 6.5 earthquake, except for the most stringent limit Ld_1 = 0.4 m where P_f is only about 10%. Increasing the earthquake magnitude to M_w = 6.75 results in slightly higher probabilities of failure where P_f is about 20% for r = 3 km with the moderate limit of Ld_2 = 0.7 m and for r = 6 km with the most stringent limit of Ld_1 = 0.4 m. For r = 3 km with Ld_1 = 0.4 m, it jumps to 80%. The probabilities of failure significantly increase when the earthquake magnitude is increased to M_w = 7.0 and particularly to 7.25. For M_w = 7.0, at distances $r \geq 3$ km, the moderate (Ld_2 = 0.7 m) and least stringent limit (Ld_3 = 1.0 m) can successfully be met. But, particularly in the close vicinity of the fault (r = 3 km), the probabilities of failure are rather high with P_f reaching up to 90% for Ld_1 = 0.4 m and 30% for Ld_3 = 1.0 m. For M_w = 7.25, it can be said that the probabilities of failure are at acceptable levels for r = 9 km and for the least stringent limit only, where P_f does not exceed 5%. But for all other cases, the probabilities of failure are unacceptably high reaching up to 100% at r = 3 km and for the most stringent limit.

6.3. Performance tests

The discussion of the results in the previous section presents that the probabilities of failure show different sensitivity to the superstructure flexibility, earthquake magnitude, and the closest distance to the fault depending on the seismic response type, i.e. peak floor acceleration, peak base displacement, or peak drift ratio. Moreover, there exist three different performance limits defined for each seismic response parameter and the combinations of different performance limits may be

Table 3
The performance limits defined for the performance tests.

	Group 1			Group 2			Group 3		
	Test 1	Test 2	Test 3	Test 4	Test 5	Test 6	Test 7	Test 8	Test 9
La (m/s^2)	≤3	≤3	≤3	≤5	≤5	≤5	≤10	≤10	≤10
Ld (cm)	≤40	≤70	≤100	≤40	≤70	≤100	≤40	≤70	≤100
Ldr (–)	≤0.0025	≤0.05	≤0.01	≤0.0025	≤0.005	≤0.01	≤0.0025	≤0.005	≤0.01

required for different situations. In order for the semi-active seismic isolation system to be reliable, it has to protect the structural integrity, structural/non-structural elements and the vibration-sensitive contents, which requires that all performance limits defined for all seismic response parameters be met simultaneously.

Table 3 lists nine different performance tests incorporating combinations of different performance limits on peak top floor accelerations (La_1, La_2, and La_3), peak inter-story drift ratios (Ldr_1, Ldr_2, and Ldr_3), and peak base displacements (Ld_1, Ld_2, and Ld_3). Tests are grouped in three: Peak acceleration limit in Group 1 (Tests 1, 2, and 3) is the most stringent (3 m/s^2), in Group 2 (Tests 4, 5, and 6) is moderate (5 m/s^2) and in Group 3 (Tests 7, 8, and 9) is the least stringent. Tests in each group are then sorted in the order of decreasing stringency in terms of peak base displacement performance limits (40, 70 and 100 cm) and peak inter-story drift ratio performance limits (0.0025, 0.005 and 0.01). Thus, the most stringent, the moderate, and the least stringent tests are Test 1, Test 5, and Test 9.

In order to lay out a wide spectrum of reliability levels considering different performance criteria for typical benchmark buildings of different number of stories with semi-active isolation systems, Fig. 12 presents performance test results in terms of the reliability of the 3-story (rigid superstructure) and 9-story (flexible superstructure) semi-actively isolated buildings for varying closest fault distances and different earthquake moment magnitudes, where the reliability (R) is defined as

$$R = 1 - P_f \tag{18}$$

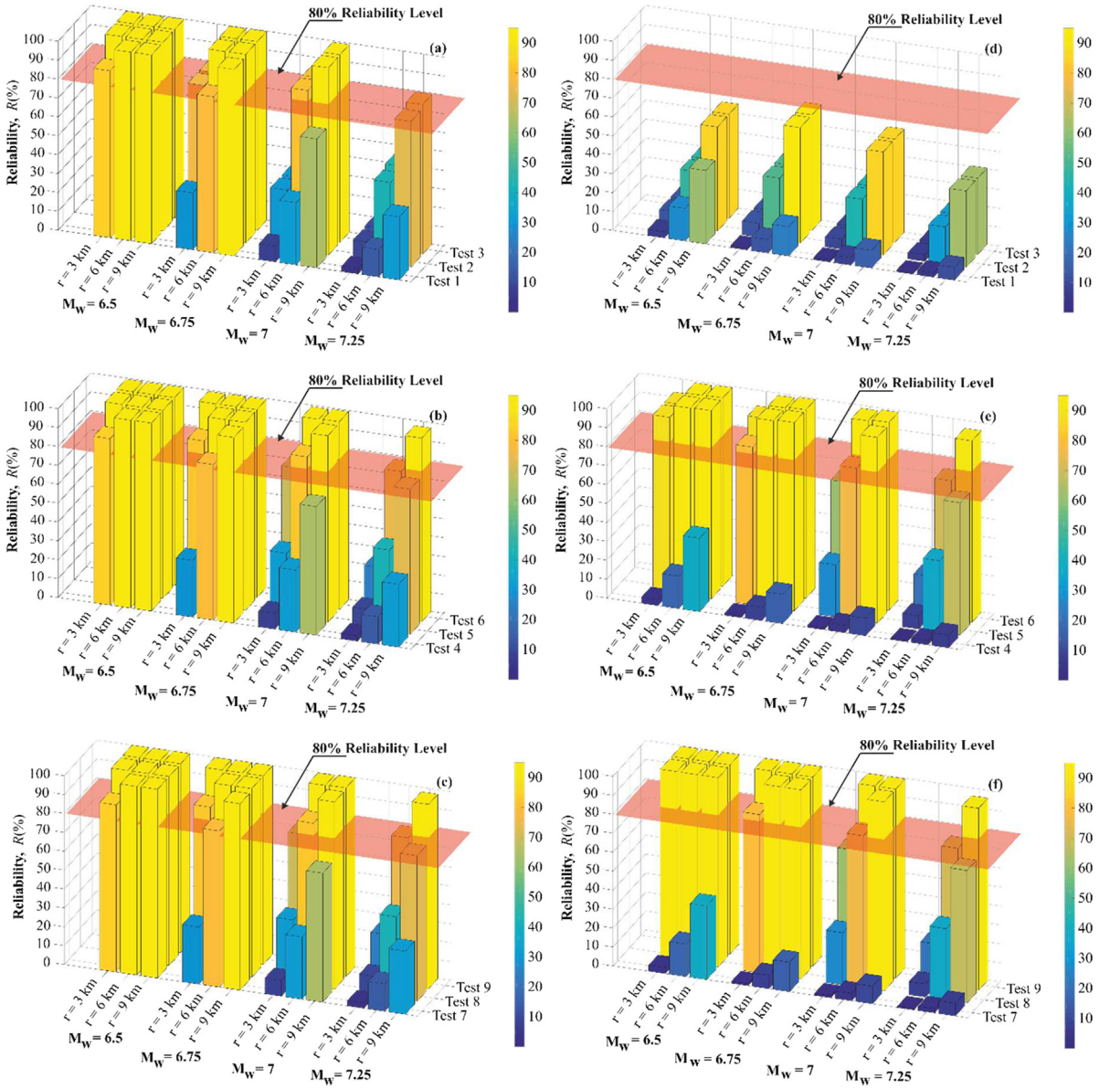

Fig. 12. Reliabilities of the semi-actively isolated buildings: the 3-story (left column) and 9-story (right column).

Although different levels of reliability (95%, 90%, etc.) may be required for different seismic isolation projects, a reliability level of 80% can be viewed as a nominally acceptable level and Fig. 12 will be assessed based on this assumption.

Group 1: This most stringent group represents the performance goals set for buildings with contents very sensitive to vibrations, such as microchip production facilities, and data centers where floor accelerations are required not to exceed 3 m/s^2. Among this group, Test 1 is the most stringent one which is included in this study to determine whether it is theoretically possible to meet such criteria. Otherwise, Test 2 and 3 include more practical expectations in terms of peak inter-story drift and peak base displacement performance limits. At first glance, it is seen Fig. 12(d) that all reliability levels are below 80%, which shows that regardless of the other criteria, 9-story building cannot meet an acceleration performance limit of 3 m/s^2. But 3-story building (Fig. 12(a)) shows success at all closest fault distances under moderate earthquakes (M_w = 6.5 and 6.75) in Tests 2 and 3 where reliability levels are above 80%. For large magnitude earthquakes (M_w = 7.0 and 7.25), reliability levels are still above 80% at fault distance of 9 km but drop below this level for closer fault distances and particularly for the M_w = 7.25 earthquake. It is also very interesting to see that 3-story building meets even the criteria of the most stringent test, Test 1, at all fault distances under moderate earthquakes (M_w = 6.5 and 6.75) except for M_w = 6.75, r = 3 km. But for larger earthquakes (M_w = 7.0 and 7.25), reliability levels under Test 1 drops below 80% at all fault distances even for the 3-story building.

Group 2: This median group represents the performance goals set for special-purpose buildings such as laboratories, hospitals, etc. which may house typical vibration-sensitive contents and thus the floor accelerations are required not to exceed 5 m/s^2. And in Test 5, which is the median of this group, the peak inter-story drift ratios are limited to the 0.005 typically set for special-purpose seismically isolated buildings so that the structural system remains essentially elastic. The base displacement is limited to 70 cm which both limits the P-delta effect on the isolators and the seismic gap to be left around the building. It is seen from Fig. 12(b) and (e)-Test 5 that both 3-story and 9-story buildings still show quite high performance for moderate earthquakes (M_w = 6.5 and 6.75) at all fault distances as the reliabilities are all above 80%. But for larger earthquake magnitudes (M_w = 7.0 and 7.25) and fault distances closer than 6 km, reliabilities drop below 80%. For the largest earthquake and the closest fault distance (M_w = 7.25, r = 3 km) the reliability is on the order of 10%. Reliabilities obtained in a less stringent test, Test 6, are close to but slightly higher than those obtained in Test 5. But for a more stringent test, Test 4, reliabilities are much lower than those obtained in Test 5: For the 3-story building, they are all below 80% for large magnitude earthquakes (M_w = 7.0 and 7.25) at all fault distances and for the moderate earthquake M_w = 6.75 at r = 3 km. For the 9-story building, all reliability levels for all earthquake magnitudes and at all fault distances are below 80% and all are much lower than those obtained for 3-story building, which shows that the peak inter-story drift ratio performance limit of 0.0025 is too stringent to meet for the 9-story building (flexible superstructure).

Group 3: This least stringent group represents the performance goals set for a residential building which does not house any vibration-sensitive content so that the floor accelerations up to 10 m/s^2 can be accepted. And in Test 9, the peak inter-story drift ratios are limited to the typical code limit of 0.01 set for seismically isolated buildings and the peak base displacement is limited to 100 cm which is a physically attainable value for rubber isolators. It is seen from Fig. 12(c) and (f)-Test 9 that both 3-story and 9-story buildings show a very high performance in these tests, reaching the reliability of 100% for moderate earthquakes (M_w = 6.5 and 6.75) for all fault distances. Although for larger earthquake magnitudes at short fault distances reliabilities drop, they are still close to 80%, except for the largest earthquake and closest fault distance (M_w = 7.25, r = 3 km) where the reliability is on the order of 20%. As the peak base displacement and peak inter-story drift ratio performance limits are tightened (Test 7 and 8), the reliability of the semi-active isolation system drops below 80%, in particular for large magnitude earthquakes (M_w = 7.0 and 7.25) and for distances closer than 6 km except for M_w = 7.0, r = 6 km. Also, the reliability levels of 9-story building are close to those of 3-story building for Tests 8 and 9 but significantly lower for Test 7, which means the peak inter-story drift ratio performance limit of 0.0025 is too stringent to meet for the 9-story (flexible superstructure) building whereas it can be met by the 3-story (rigid superstructure) building unless large magnitude earthquakes (M_w = 7.0 and 7.25) at very close fault distances ($r \leq 6$ km) are considered.

7. Conclusions

Semi-active seismic isolation systems reduce large isolation system displacements that may occur in the case of near-fault earthquakes without significantly increasing the floor accelerations that may become a concern if passive dampers are used to provide supplemental damping. Furthermore, they do not require large external power or cause instability problems, which may be a concern if active control used. In this study, the effectiveness of semi-active isolation in protecting vibration-sensitive equipment and structural integrity considering potential variations in the mechanical properties of semi-active devices and/or seismic isolators as well as those in the earthquake parameters is examined. A methodology that employs the generation of synthetic near-fault earthquakes and Monte-Carlo Simulations is introduced, which is used to determine the reliability of 3-story (rigid superstructure) and 9-story (flexible superstructure) benchmark buildings with semi-active isolation systems under near-fault earthquakes of various magnitudes and closest fault distances. Reliability plots that present a wide spectrum of reliability levels considering different practical performance criteria for the benchmark structures representing typical buildings with semi-active isolation systems of different superstructure flexibilities for varying fault distances and earthquake magnitudes are expected to provide useful information for practicing engineers. Other main outcomes of this study can be summarized as follows:

(1) Cumulative distribution function plots have shown that the seismic responses of semi-actively isolated buildings can vary significantly due to the uncertainties in the mechanical parameters of semi-active isolation system elements and the uncertainties in the earthquake parameters.
(2) As a general trend, it is seen that the probabilities of failure significantly increase as the moment magnitude increases and the fault distance decreases.
(3) The probabilities of failure in terms of peak floor accelerations and peak inter-story drift ratios are much higher for semi-actively isolated buildings with flexible superstructures compared to those with rigid superstructures, while the probability of failure in terms of peak base displacements is similar for both.
(4) The probability of failure profiles along the height of the semi-actively isolated buildings in terms of peak floor accelerations revealed that the probabilities of failure are much lower at mid-floors compared to the lower-most and the upper-most floors of buildings with flexible superstructures whereas they are pretty much the same at all floors of buildings with rigid superstructures.
(5) The inter-story drift ratio is an indicative response parameter regarding the safety of structural and non-structural elements. Although ASCE 7–10 limit of 0.01, for which accidental yielding may occur, can easily be met by semi-actively isolated buildings both with rigid and flexible superstructures, 0.005 limit corresponding to the elastic behavior of the superstructure is exceeded for the flexible superstructure when $M_w \geq 7.0$ and $r \leq 6$ km. This suggests that semi-actively isolated buildings with flexible superstructures should be analyzed for nonlinear effects in the superstructure when subjected to near-fault earthquakes. 0.0025 limit which may be set for avoiding even minor damages to brittle non-structural members (e.g., plaster cracks, window damages, etc.) can be met by rigid superstructures for $M_w \leq 7.0$ but cannot be met by flexible superstructures even for a moderate earthquake $M_w = 6.5$ within the near-fault region ($r \leq 9$ km).
(6) For semi-actively isolated buildings *with contents very sensitive to vibrations* where floor accelerations are required not to exceed 3 m/s^2, such as microchip production facilities, data centers, etc. it is observed that those with flexible superstructures cannot meet such an acceleration performance limit in the near-fault region ($r \leq 9$ km) either for moderate or high earthquake magnitudes as reliabilities turned out to be below 80%. But for those with rigid superstructures are shown to be reliable in the near-fault region ($r \leq 9$ km) in case of moderate ($M_w = 6.5$ and 6.75) earthquakes as long as the inter-story drift and base displacement performance limits are set as sensible, i.e. 0.005 and 70 cm, respectively. For larger earthquake magnitudes ($M_w = 7.0$, 7.25), reliability levels are still above 80% at the fault distance of 9 km but drop below this level for closer fault distances.
(7) For semi-actively isolated special-purpose buildings such as laboratories, hospitals, etc. with *typical vibration-sensitive contents* where the floor accelerations are required not to exceed 5 m/s^2, it is observed that in case the inter-story drift and base displacement performance limits are set as 0.005 and 70 cm, respectively, which are typically expected performances, those with both rigid and flexible superstructures have proven to be reliable for moderate earthquakes ($M_w = 6.5$ and 6.75) for all fault distances considered in this study. But for larger earthquake magnitudes ($M_w = 7.0$ and 7.25) and fault distances closer than 6 km, reliabilities are below 80%.
(8) For semi-actively isolated residential buildings *without any vibration-sensitive contents* where floor accelerations up to 10 m/s^2 can be accepted, it is observed that in case the peak inter-story drift ratio and peak base displacement performance limits are set as 0.01 and 100 cm, which are the typical code limit and physically attainable limit of rubber isolators, respectively, those with both rigid and flexible superstructures have proven to be reliable for all earthquake magnitudes ($M_w < 7.25$) at all near-fault distances ($r \leq 9$ km) considered in this study except for the largest earthquake and closest fault distance ($M_w = 7.25$, $r = 3$ km) where the reliability is about 20%.

Acknowledgements

The authors would like to thank the Faculty Member Training Program Office (ÖYP) of Istanbul University for providing financial support.

References

[1] T.H. Heaton, J.F. Hall, D.J. Wald, M.W. Halling, Response of high-rise and base-isolated buildings to a hypothetical Mw 7.0 blind thrust earthquake, Science 267 (1995) 206–211.
[2] C. Alhan, S. Oncu-Davas, Performance limits of seismically isolated buildings under near-field earthquakes, Eng. Struct. 116 (2016) 83–94.
[3] A.A. Taflanidis, G. Jia, A simulation-based framework for risk assessment and probabilistic sensitivity analysis of base-isolated structures, Earthquake Eng. Struct. Dyn. 40 (2011) 1629–1651.
[4] J.M. Kelly, The role of damping in seismic isolation, Earthquake Eng. Struct. Dyn. 28 (1999) 3–20.
[5] J.F. Hall, The role of damping in seismic isolation, Earthquake Eng. Struct. Dyn. 28 (1999) 1717–1720.
[6] C. Alhan, H. Gavin, A parametric study of linear and non-linear passively damped seismic isolation systems for buildings, Eng. Struct. 26 (2004) 485–497.
[7] F. Mazza, A. Vulcano, Nonlinear response of RC framed buildings with isolation and supplemental damping at the base subjected to near-fault earthquakes, J. Earthquake Eng. 13 (2009) 690–715.
[8] C. Alhan, H.P. Gavin, Reliability of base isolation for the protection of critical equipment from earthquake hazards, Eng. Struct. 27 (2005) 1435–1449.
[9] M. Singh, E. Matheu, L. Suarez, Active and semi-active control of structures under seismıc excitation, Earthquake Eng. Struct. Dyn. 26 (1997) 193–213.
[10] K. Yamada, T. Kobori, Fundamental dynamics and control strategies for aseismic structural control, Int. J. Solids Struct. 38 (2001) 6079–6121.
[11] K.W. Wang, Y.S. Kim, Semi-active vibration control of structures via variable damping elements, Mech. Syst. Sig. Process. 5 (1991) 421–430.

[12] M.D. Symans, M.C. Constantinou, Semi-active control systems for seismic protection of structures: a state-of-the-art review, Eng. Struct. 21 (1999) 469–487.
[13] F. Casciati, J. Rodellar, U. Yildirim, Active and semi-active control of structures - theory and applications: A review of recent advances, J. Intell. Mater. Syst. Struct. 23 (2012) 1181–1195.
[14] M.D. Symans, G.J. Madden, N. Wongprasert, Experimental study of an adaptive base isolation system for buildings, in: Proc. of 12th World Conf. on Earthquake Eng., 12WCEE, 2000.
[15] J.N. Yang, A.K. Agrawal, Semi-active hybrid control systems for nonlinear buildings against near-field earthquakes, Eng. Struct. 24 (2002) 271–280.
[16] G.J. Madden, N. Wongprasert, M.D. Symans, Analytical and numerical study of a smart sliding base isolation system for seismic protection of buildings, Comput.-Aided Civ. Inform. 18 (2003) 19–30.
[17] C. Alhan, H.P. Gavin, U. Aldemir, Optimal control: Basis for performance comparison of passive and semiactive isolation systems, J. Eng. Mech-Asce 132 (2006) 705–713.
[18] J. Da la Llera, J. Inaudi, Analysis of base-isolated buildings considering stiffness uncertainty in the isolation system, in: Proc. 5th US National Conference on Earthquake Engineering, 1994, pp. 10–14.
[19] H.W. Shenton, E.S. Holloway, Effect of stiffness variability on the response of isolated structures, Earthquake Eng. Struct. Dyn. 29 (2000) 19–36.
[20] A.C. Thompson, A.S. Whittaker, G.L. Fenves, S.A. Mahin, Property modification factors for elastomeric seismic isolation bearings, in: Proceedings of the 12th World Conference on Earthquake Engineering, Auckand New Zealand, 2000.
[21] I. Politopoulos, H.K. Pham, Sensitivity of seismically isolated structures, Earthquake Eng. Struct. Dyn. 38 (2009) 989–1007.
[22] H.J. Pradlwarter, G.I. Schueller, U. Dorka, Reliability of MDOF-systems with hysteretic devices, Eng. Struct. 20 (1998) 685–691.
[23] E.M. Guneyisi, G. Altay, Seismic fragility assessment of effectiveness of viscous dampers in R/C buildings under scenario earthquakes, Struct. Saf. 30 (2008) 461–480.
[24] O. Curadelli, Seismic reliability of spherical containers retrofitted by means of energy dissipation devices, Eng. Struct. 33 (2011) 2662–2667.
[25] J.I. Colombo, J.L. Almazan, Seismic reliability of continuously supported steel wine storage tanks retrofitted with energy dissipation devices, Eng. Struct. 98 (2015) 201–211.
[26] S. Chakraborty, R. Debbarma, Robust optimum design of tuned liquid column damper in seismic vibration control of structures under uncertain bounded system parameters, Struct. Infrastruct. Eng. 12 (2015) 592–602.
[27] H. Gazi, Probabilistic behavior of semismically isolated buildings under earthquake loads, Istanbul University, İstanbul, 2015, PhD Dissertation.
[28] J.G. Chase, L.R. Barroso, S. Hunt, The impact of total acceleration control for semi-active earthquake hazard mitigation, Eng. Struct. 26 (2004) 201–209.
[29] A.M. Aly, R.E. Christenson, On the evaluation of the efficacy of a smart damper: a new equivalent energy-based probabilistic approach, Smart Mater. Struct. 17 (2008) 11.
[30] S. Nagarajaiah, A.M. Reinhorn, M.C. Constantinou, 3D-BASIS-nonlinear dynamic analysis of three-dimensional base isolated structures: Part II, 1991.
[31] H. Gavin, C. Alhan, N. Oka, Fault tolerance of semiactive seismic isolation, J. Struct. Eng.-Asce 129 (2003) 922–932.
[32] S. Öncü-Davas, Probabilistic Behavior of Buildings with Semi-active Seismic Isolation Systems under Earthquake Loads, Istanbul University, PhD Dissertation (unpublished).
[33] MATLAB, The MathWorks Inc., 2016.
[34] Y. Park, Y. Wen, A. Ang, Random vibration of hysteretic systems under bi-directional ground motions, Earthquake Eng. Struct. Dyn. 14 (1986) 543–557.
[35] R. Bouc, Forced vibration of mechanical systems with hysteresis, Proceedings of the fourth conference on non-linear oscillation, Prague, Czechoslovakia, 1967.
[36] Y.-K. Wen, Method for random vibration of hysteretic systems, J. Eng. Mech. Division 102 (1976) 249–263.
[37] M. Dicleli, S. Buddaram, Equivalent linear analysis of seismic-isolated bridges subjected to near-fault ground motions with forward rupture directivity effect, Eng. Struct. 29 (2007) 21–32.
[38] A. Tena-Colunga, J.L. Escamilla-Cruz, Torsional amplifications in asymmetric base-isolated structures, Eng. Struct. 29 (2007) 237–247.
[39] C.P. Providakis, Effect of supplemental damping on LRB and FPS seismic isolators under near-fault ground motions, Soil Dyn. Earthquake Eng. 29 (2009) 80–90.
[40] V.A. Matsagar, R.S. Jangid, Influence of isolator characteristics on the response of base-isolated structures, Eng. Struct. 26 (2004) 1735–1749.
[41] D.C. Vu, I. Politopoulos, S. Diop, Relaxation base seismic isolator, Earthquake Eng. Struct. Dyn. 45 (2016) 2027–2037.
[42] M. Crosby, R. Harwood, D. Karnopp, Vibration control using semi-active force generators, J. Eng. Ind. 96 (1974) 619–626.
[43] C. Alhan, H. Gazi, H. Kurtuluş, Significance of stiffening of high damping rubber bearings on the response of base-isolated buildings under near-fault earthquakes, Mech. Syst. Sig. Process. 79 (2016) 297–313.
[44] N. Makris, Rigidity-plasticity-viscosity: can electrorheological dampers protect base-isolated structures from near-source ground motions?, Earthquake Eng Struct. Dyn. 26 (1997) 571–592.
[45] N. Makris, S.P. Chang, Effect of viscous, viscoplastic and friction damping on the response of seismic isolated structures, Earthquake Eng. Struct. Dyn. 29 (2000) 85–107.
[46] B. Alavi, H. Krawinkler, Consideration of near-fault ground motion effects in seismic design, in: Proceedings of the 12th World Conference on Earthquake Engineering, 2000, pp. 8.
[47] A. Agrawal, W. He, A close-form approximation of near-fault ground motion pulses for flexible structures, in: ASCE Engineerıng Mechanics Conference, 2002.
[48] C. Menun, Q. Fu, An analytical model for near-fault ground motions and the response of SDOF systems, in: Proceedings, 7th US National Conference on Earthquake Engineering, Boston, Massachusetts, 2002, pp. 21–25.
[49] G.P. Mavroeidis, A.S. Papageorgiou, A mathematical representation of near-fault ground motions, Bull. Seismol. Soc. Am. 93 (2003) 1099–1131.
[50] W.L. He, A.K. Agrawal, Analytical model of ground motion pulses for the design and assessment of seismic protective systems, J. Struct. Eng.-Asce 134 (2008) 1177–1188.
[51] J.F. Hall, T.H. Heaton, M.W. Halling, D.J. Wald, Near-source ground motion and its effects on flexible buildings, Earthquake Spectra 11 (1995) 569–605.
[52] P. Somerville, Development of an improved representation of near fault ground motions, in: SMIP98 Seminar on Utilization of Strong-Motion Data, 1998.
[53] A. Rodriguez-Marek, Near-Fault Seismic Site Response, University of California, Berkeley, 2000.
[54] H. Perros, Computer Simulation Techniques: the definitive introduction!, 2009.
[55] A. Haldar, S. Mahadevan, Probability, Reliability and Statistical Methods in Engineering Design, John Willey & Sons, 2000.
[56] C. Alhan, H. Gazi, Bringing probabilistic analysis perspective into structural engineering education: use of monte carlo simulations, Int. J. Eng. Educ. 30 (2014) 1280–1294.
[57] C. Alhan, F. Sahin, Protecting vibration-sensitive contents: an investigation of floor accelerations in seismically isolated buildings, Bull. Earthq. Eng. 9 (2011) 1203–1226.
[58] T.L. Karavasilis, C.-Y. Seo, Seismic structural and non-structural performance evaluation of highly damped self-centering and conventional systems, Eng. Struct. 33 (2011) 2248–2258.
[59] R.S. Jangid, Optimum lead-rubber isolation bearings for near-fault motions, Eng. Struct. 29 (2007) 2503–2513.
[60] ASCE, Minimum Design Loads for Buildings and Other Structures, 2010.
[61] P. Pan, D. Zamfirescu, M. Nakashima, N. Nakayasu, H. Kashiwa, Base-isolation design practice in Japan: Introduction to the post-kobe approach, J. Earthquake Eng. 9 (2005) 147–171.